Chapter 2
The ANTARES Detector

The ANTARES[1] detector (Ageron et al. 2011) is a pilot project to demonstrate that underwater neutrino telescopes are feasible and that they can operate for several years in the sea water at great depths. The ANTARES detector is located near Toulon, France. The coordinates are $42°50'$ N and $6°10'$ E. Its location makes it sensitive to a large part of the southern sky, including the Galactic Centre region. The detector is located at a depth of 2475 m on the Mediterranean seabed. There is a large plateau in this place (several tens of km^2 with a depth change less than 200 m, Fig. 2.1) which is promising for the further project extension.

In this chapter a general description of the detector design and its operation is given. In particular, characteristics of the used PMTs and the optical modules containing them are described in details. Measurements of the PMT characteristics and simulation of the optical module, which have been part of this thesis work, are essential for the complete detector simulation. The detector simulation itself will be described in Chap. 3.

2.1 Detector Design

The underwater Cherenkov neutrino telescope detector should fulfil the following requirements:

- Due to the very low flux of the high-energy neutrinos from astrophysical sources and to the small neutrino interaction cross-section, a large instrumented volume is required.
- Optimised light detection efficiency and high timing accuracy are needed for the detector elements. The detection units should be capable to detect single photons with a nanosecond precision.

[1] Astronomy with a Neutrino Telescope and Abyss environmental RESearch.

V. Kulikovskiy, *Neutrino Astrophysics with the ANTARES Telescope*,
Springer Theses, DOI 10.1007/978-3-319-20412-3_2

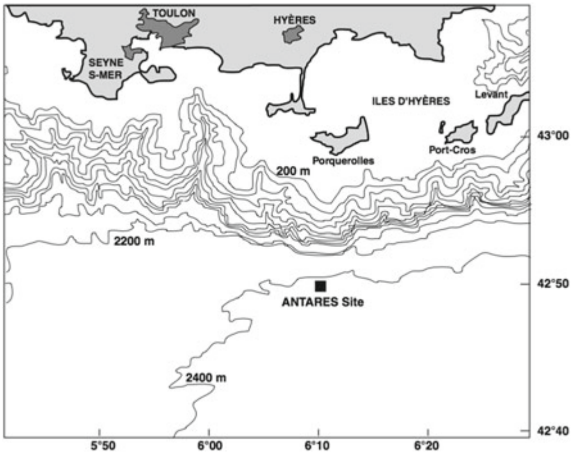

Fig. 2.1 Depth contour plot near the ANTARES site. Each profile line corresponds to 200 m depth change. This image is taken from Palioselitis (2012)

- High pressure resistance. The detector depth of more than 2 Km must be considered to decrease the atmospheric muon rate. The detector components must withstand also additional stress during the installation (shocks, exposure to sunlight etc.).
- The lifetime should be greater than 10 years. The accessibility to the detector is difficult and expensive due to a great depth. Reliability of the components should be high.

To meet these requirements large spherical photomultiplier tubes (10$''$ radius) were used for the light detection. Their choice is discussed in the next section. For the protection, each PMT and its associated electronics (power base) is housed in a pressure-resistant glass sphere to construct an optical module (OM). There are 885 OMs used in the ANTARES detector.

The arrangement of the OMs in space was optimised by the mean of simulation to have the best neutrino detection efficiency which consists of the effective detection volume and the angular resolution for the tracks. The optimal distances between OMs are correlated with the absorption length in water (maximum is about 60 m as it is described in Sect. 3.3.1). Time coincidence conditions between close OMs (< 1 m) allows to reduce an optical background in the sea water (Sect. 3.3.4). The Fig. 2.2 shows the detector configuration, constituted of OM trios distributed on vertical lines.

The lines are flexible structures attached to the sea bottom by a heavy anchor and kept in tension by a buoy on the top of each line. There are 12 lines with a distance of 60–65 m between them. Any line can be deployed independently from others and released to the surface for maintenance. This simplifies operations at great depth. The lines are connected to the common junction box with 80 Km cable connecting the junction box to the shore station (La Seyne-sur-Mer) where the ANTARES control room is located. Each line (except one[2]) has 25 storeys.

[2]The last line has hydrophones instead of OMs in the five top storeys.

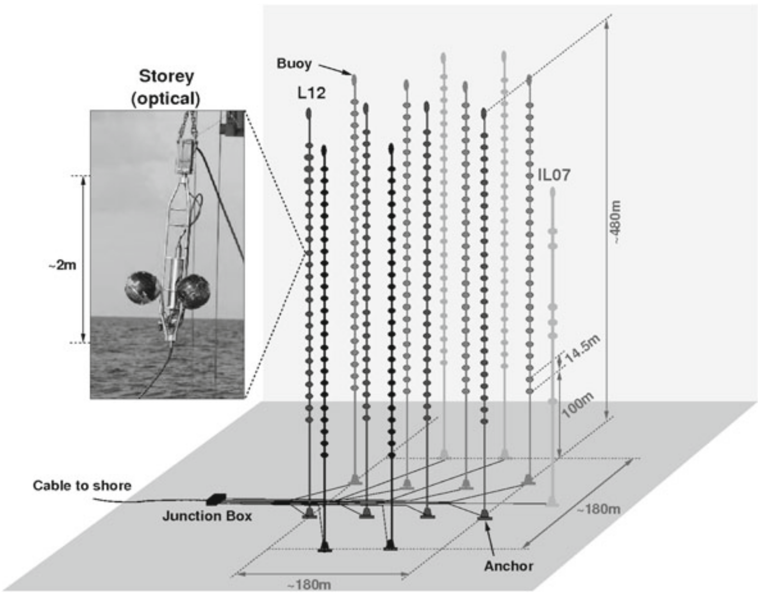

Fig. 2.2 Schematic view of the ANTARES 12-line detector. The image is taken from Palioselitis (2012)

The storey is a mechanical structure to place three OMs to point downwards at 45° with respect to the vertical. OMs are downwards oriented to optimise the upgoing particles detection. Also this orientation allows to protect the OM sensitive area from the sedimentation. The storeys are separated by 14.5 m on the line connected with an electro-optical cable. The first storey is placed 100 m above the anchor. This distance is the minimal distance from the ground where the Čerenkov cone from the up-going particles is developed.

In the following sections the key components of the detector are described in details paying more attention to the PMTs and OMs for which I performed different studies during this thesis.

2.1.1 Photomultipliers

In PMTs arriving photons are converted to electrons via photoelectric effect on the thin metal layer of the so-called photocathode. The electrons are then carried to the stack of the dynode plates with a high voltage between them. Accelerated by the electric field in the tube, the electrons knock out more electrons on each dynode. The gained cascade of the electrons after a stage of several dynodes is sufficient to be seen on the collecting anode even for a single arrived photon. These processes are schematically shown in Fig. 2.3. A typical PMT anode signal due to the single

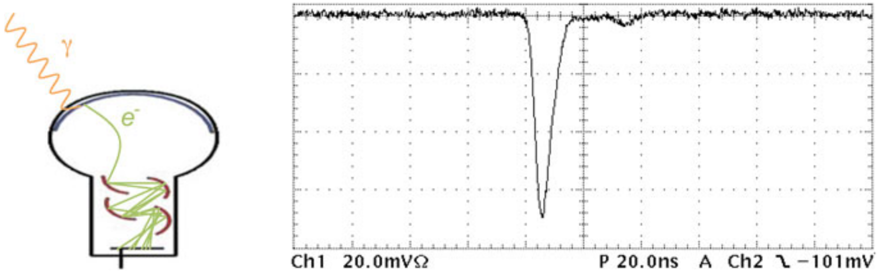

Fig. 2.3 Scheme of detection of a photon by a PMT (*left*). The photon (*yellow*) arrives to the photocathode (*blue*) where it knocks out electron (*green*) which in turn is accelerated in the electric field between the photocathode and the dynode stack (*red*). On each dynode plate there is a chance to knock out additional electrons which are accelerated to the next dynode plate by an electric field between the dynodes. An example of a PMT response to a single photon exposure (*right*)

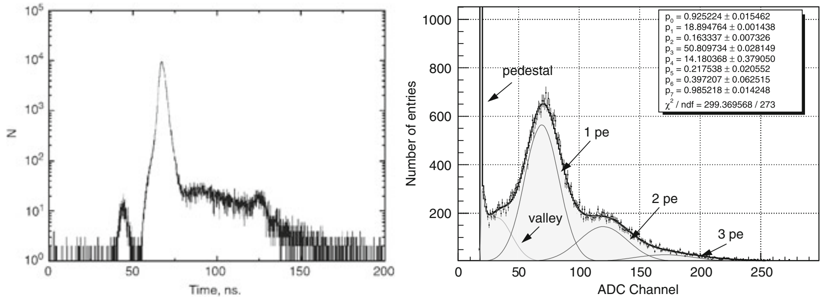

Fig. 2.4 Example of a single photoelectron transit time distribution (*left*). The image is taken from Lubsandorzhiev et al. (2006). Example of a charge distribution expressed in number of digitiser channels, which are proportional to a charge in Coulombs (*right*). This distribution is fitted with several Gaussian functions which correspond to the different number of photoelectrons, emitted from the photocathode. The image is taken from Aguilar et al. (2005)

photon arrival is shown in the same figure. This signal is normally digitised as a time at which the signal amplitude becomes higher than a threshold (typically, 1/3 of the peak) and the total charge integrated in the time window where the signal stays over the threshold (slightly extended to contain a whole signal from a single photon arrived).

A typical time distribution of the detected hits as a response to arriving single photons is shown in Fig. 2.4. The main peak with an approximately Gaussian distribution is seen. The so-called transit time spread (TTS) is referred in following to the full width at half-maximum (FWHM) of this transit time distribution. Additional peaks due to prepulses and delayed pulses are also present. Their origin is discussed in Sect. 2.1.3.

A typical charge distribution for single photons has a Gaussian shape (Fig. 2.4) and it corresponds to the number of electrons gained on the dynode stack (gain). The total charge which corresponds to the mean of this distribution scales linearly for the number of photons simultaneously arrived to the PMT. This makes efficient to express the charge as a number of photoelectrons (p.e.) by dividing the charge by the mean charge value which corresponds to the single photon. Digitised anode signal is called "hit" in following.

Photocathode is typically done using alkali metals and it operates in the vacuum. Probability of a photon to produce a photoelectron is called quantum efficiency and it is about 20–40 % for modern photocathodes. The photocathode should be negatively charged. Electron emission happens due to the photoelectric effect and the electrons escape the photocathode on the opposite site from the arrived photon and then they are driven away by the initial kinetic energy and the electric field.

In modern experiments PMTs are widely used thanks to the high amplitude output (comparing to photodiodes), sensitivity to single photons, linear response to different amount of arrived photons and good timing characteristics. A large variety of PMTs with different sizes and shapes of photocathode are available commercially. PMTs with a spherical photocathode have the best timing resolution, as the photoelectrons cover almost the same distance to the first dynode from any point on the photocathode.

PMTs with a large photocathode are more sensitive to the magnetic fields (for example, the Earth's magnetic field) as the electrons are more deflected on greater distances. The magnetic shielding is important for such PMTs. PMTs have vacuum inside the bulb to have a better electron collection efficiency and reduce the spurious pulses arriving from the ionised gas. Together with the thin glass in front of the photocathode this makes them a very fragile device. Photocathode could be damaged by a high light flux and also photocathode material can degrade with a time (ageing).

2.1.2 PMT Choice

The PMT model was chosen during research and development phase of the ANTARES project (Aguilar et al. 2005). Several requirements for the PMT choice should be satisfied:

Size The previously mentioned requirements of the detector size can be satisfied if the total density of the photomultipliers is low (10^{-4} PMT/m^3) to reduce the cost of mechanics. These in turn leads to the fact that the number of detectable photons produced by muons is very low for each detection unit. This requires a large detection area for each unit. Simulation shows that the geometrical area of the PMT should be more than 400 cm^2 if the photocathode quantum efficiency $\geq$20 % is considered.

Timing The time resolution has an impact on the reconstructed muon angular resolution. The ANTARES experiment aimed absolute time calibration better than 1 ns. The timing uncertainty due to the jitter of the PMT response should also remain of the order of 1 ns, in order not to degrade significantly the angular resolution. It was decided that TTS should not exceed 3 ns (Aguilar et al. 2005).

Gain The noise level of the electronic circuit used to digitise PMT pulses requires a single photoelectron (SPE) amplitude to be of the order of 50 mV on a 50 Ω load (Feinstein 2003). This requires the photomultiplier gain to be at least 5×10^7. For the absolute calibration of the telescope, it is necessary to be able to properly isolate a single photoelectron from the pedestal. This requires peak-to-valley ratio (P/V) to be at least 2, as computed from the charge spectrum. The charge resolution should be less than 40 %.

Noise The optical background in the sea water at ANTARES site is about 60 kHz for a 10″ PMT (see Sect. 3.3.4). The dark count rate should be negligible comparing to this rate so the maximum dark count rate <10 kHz is required. The dark count rate includes the PMT noise (spontaneous electron emission from a photocathode and dynodes and other processes) and the radioactive decay in the glass and the optical gel of the OM (^{40}K decay mainly).

A signal from PMTs can be affected by different spurious pulses. Basically one distinguishes prepulses, which arrive before the main pulse together or instead of it, delayed pulses which arrive with a 10–100 ns delay instead of the main pulse, afterpulses which arrive together with the main pulse in several time windows: 10–100 ns (afterpulses type 1) or 100 ns–16 μs (afterpulses type 2). The detailed study with the description of the physical process involved for these pulses is done in Sect. 2.1.3.

A large variety of PMT models have been tested and characterised taking into account the constraints listed above. At the end of the tests, the Hamamatsu R7081-20 model was chosen for the ANTARES detector. The full sample of the delivered PMTs (912) has been tested with a dedicated test bench in order to calibrate the sensors and to check the compliance with the specifications. The number of rejected tubes was low (17, their peak/valley ratio being too low), these tubes were replaced by the manufacturer (Ageron et al. 2011).

The ageing was studied with a test setup which simulates the optical background in the sea. The total charge of 500 C, corresponding to 10 years in the sea was collected by each of the three tested PMTs. The LED's pulsers are programmed to emit light continuously with a rate of 500 kHz and bursts of 5 MHz lasting 0.1 s every second to simulate extreme conditions of the optical background in sea water (discussed in details in Sect. 3.3.4). Over the first 100 days, all three PMTs showed an increase of 50–70 % in gain, before they level off. This phenomenon corresponds to the running-in phase, rather than the ageing. All other important energy and timing properties of the PMTs (P/V, energy resolution and TTS) were stable over the test period. The dark count rate remained also stable with time. However, the afterpulses type 2 rate showed an increase (around 30 %) during the test, possibly caused by the fact that these pulses are usually due to the ionised gas, which quantity increases with time (Aguilar et al. 2005).

The selected PMTs fulfil the requirements. For my thesis I performed several measurements with one of these PMTs to get acknowledged with the principles of PMT work and to insert measured data to the simulation of the ANTARES detector.

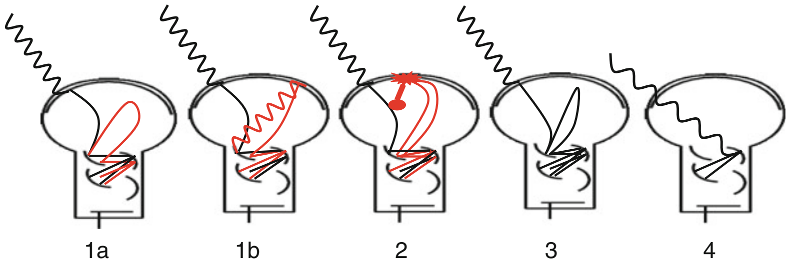

Fig. 2.5 Afterpulse type 1 (*1a, 1b*), afterpulse type 2 (*2*), late pulse (*3*) and prepulse (*4*) origins in a PMT

2.1.3 PMT Characteristics Measurement

Since the track reconstruction is based on the light arrival to the PMT it is necessary to know its transit time spread precisely to be used in the detector simulations later. This transit time spread is affected by several processes. Also, in addition to the normally detected photon signal, correlated pulses may appear with some delay. The spurious pulses affecting TTS or appearing after the normal pulse may be summarised as following (Fig. 2.5):

1. **Afterpulses type 1**: they appear in the first 80 ns after the main pulse and can be produced by the luminous reaction on the dynodes while bombarded by electrons or by the electrons escaped from the dynode in the direction to the photocathode.
2. **Afterpulses type 2**: appear in 80 ns–16 μs interval after the main pulse due to the ionisation of the phototube gas by the photoelectron. Different ions give different contributions to the afterpulses time distribution (H^+, He^+ and heavy ions CH_4^+, O^+, N_2^+, O_2^+, Ar^+ and CO_2^+).
3. **Late pulses**: a primary photoelectron suffers from the elastic or inelastic scattering in the first dynode without a secondary electrons emission, it turns towards the photocathode making a loop and only after it creates a cascade of electrons in the dynodes. The arrival time of the hit will be delayed.
4. **Prepulses**: they appear due to the direct photoelectron emission on the dynodes from the photons which passed the photocathode without an interaction. Due to this, the main pulse arrives earlier and with a smaller charge.

In order to study these processes the following test setup was developed. At first, a bare R7081-20 10″ PMT with the same power base as in the ANTARES detector was used. The PMT was located in a black light tight box with a feed through for power supply and anode signal output. In the same box a Hamamatsu Picosecond Light Pulser PLP10-044C was located. This laser had a wavelength of 440 nm, a pulse width of few picoseconds and a tunable frequency from 1 Hz to 1 MHz. The beam output was connected via an optical fibre to an attenuator and then to a collimator to illuminate the PMT photocathode as shown in Fig. 2.6. A compact diffuser obtained sanding a thin plexiglas sheet ensured not a perfect but an acceptable uniform illumination

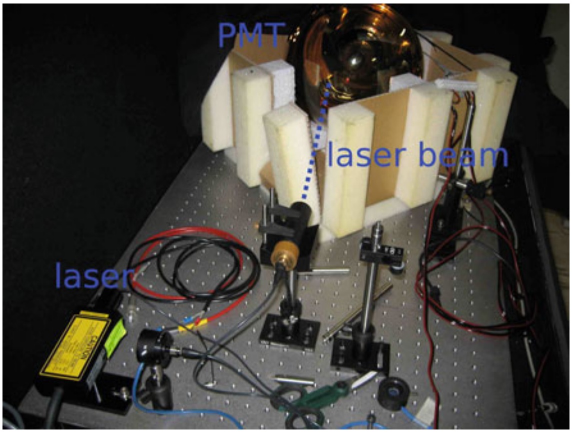

Fig. 2.6 Photograph of the experimental setup used for the ANTARES PMT studies

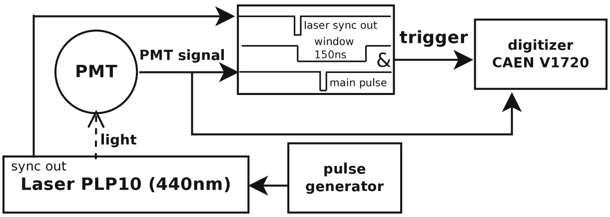

Fig. 2.7 Scheme of the acquisition system used for the ANTARES PMT studies

of the surface. The light from the laser was tuned to obtain, at the photocathode window, $\approx 10^{-2}$ photons/pulse to produce on average one signal at the PMT anode every 500 light pulses sent by the laser. In these conditions one can assume that the laser is working in the single photoelectron (SPE) mode. The data acquisition system was extremely simple. The output of the PMT anode was split to a 0.3 p.e. threshold discriminator and to a fast, 1 GHz, CAEN digitiser V1731. The output of the discriminator was stretched to 150 ns and put in coincidence with the Laser SYNC out as shown in Fig. 2.7. In order to exploit the full timing capabilities of the CAEN fast ADC, both the coincidence and the anode signals were sent respectively to channel 0 and 2 of the digitiser. Worth to notice that the logic unit output was always synchronous with respect to the laser SYNC out: the arrival time of the PMT signal was therefore measured relative to the light pulse. In practice, the coincidence NIM signal in channel 0 was used to trigger the acquisition in the following 16 μs time window. To check that this system provided the correct timing, I have sent the two outputs of the same discriminator, one delayed by a fixed quantity, to the CAEN digitiser: the obtained distribution showed a sharp peak, 1 ns FWHM, as expected. The example of the digitised pulse is shown in Fig. 2.8.

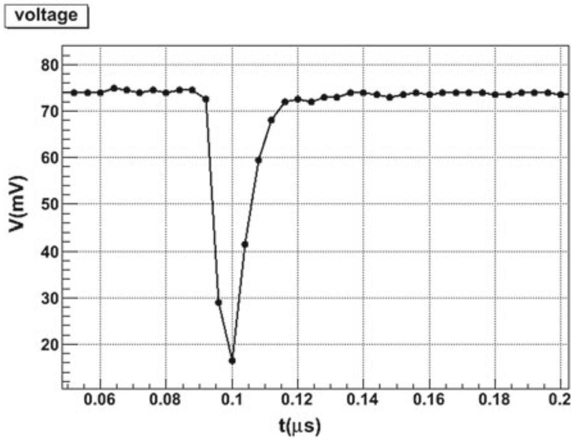

Fig. 2.8 The anode pulse as measured by the CAEN digitiser with the linear interpolation which is used for the charge calculation

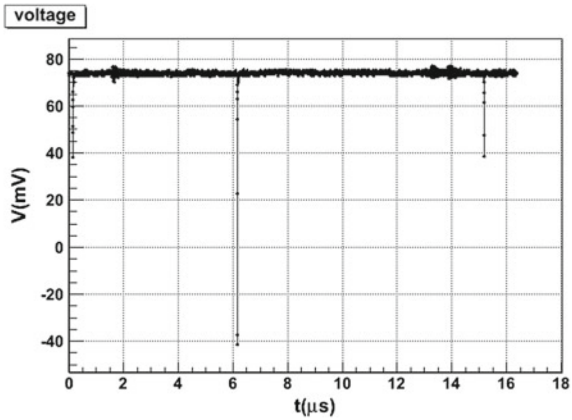

Fig. 2.9 The PMT anode output together with possible after-pulses at 6 and 15 μs from the laser pulse

A typical digitised PMT anode output is plotted in Fig. 2.9 in the 16 μs time interval. Together with the main pulse at the origin of the time axis, after-pulses are seen after 6 and 15 μs. Also some electronic noise can be seen at ~2 and ~13 μs. Sampling rate was 1 GHz and voltage was digitised in 4 mV steps. The time and charge analysis consisted of the next steps:

1. Determination of DAQ offset in the 16 μs interval and subtract it from the signal.
2. Search for all peaks and their charge by iterating time sample by time sample. When the signal is higher than 10 mV, corresponding to a threshold of about 0.2–0.3 p.e., the program looks for the presence of a peak and finds the left and right boundaries of the peak T_l and T_r where the amplitude of the signal is higher than 10 mV. The time of the maximum amplitude is considered as the time of the pulse. Two peaks within a 25 ns time interval are assigned to the same event and the time of the event is the time of the maximum of the two peaks. The charge is

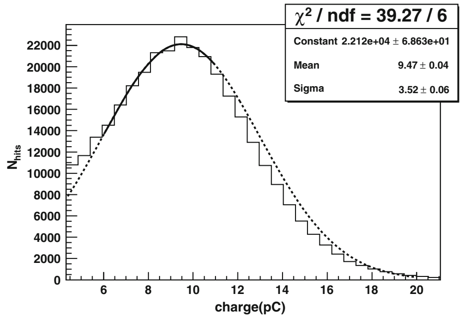

Fig. 2.10 Measured ANTARES PMT charge due to a single photon arrival

evaluated integrating the peak within the Simpson approximation from $T_l - 5$ to $T_r + 10$ ns.

3. The hits in the first 200 ns of the time window are considered as "normal" (not afterpulses). The plot of the corresponding charge distribution is shown in Fig. 2.10. The plot is well fitted with a single Gaussian distribution to prove that contributions of two or more photo electrons to the main hits are negligible. The left part at low charge is a little bit distorted due to the contribution of prepulses with low charge. The mean value of the charge of the 1 p.e. peak $\tilde{q}$ is found from the fit. After the fit is done, the charge of a hit q is divided by $\tilde{q}$ to obtain the charge in photoelectrons.

The performed measurements of TTS are shown in Fig. 2.11. The peak of the normal pulses from the laser photons is clearly evident at $t \sim 100$ ns while random background forms a plateau in accordance to the dark current measured rate of $\sim$1.6 kHz in the absence of the laser signal.

The first measurement was done with a uniform diffuse illumination and the second was done with a point like beam towards the centre of a PMT photocathode. In both cases a significant tail towards the increasing arrival times can be observed. This tail might be ascribed to an inelastic scattering of the photoelectron in the first dynode (Lubsandorzhiev et al. 2006). It is expected that this effect can be a bit larger for the uniform illumination. Also there is an additional structure at $\sim$50 ns from the main peak which is ascribed to the elastic scattering of the photoelectron. In the latter case the momentum of the scattered electron is fixed which creates a fixed delay as well. To this extent, assuming a uniform electric field of $\sim$60 V/cm at 14 cm distance between the first dynode and the photocathode, the 50 ns of the peak roughly corresponds to the "round trip" of an electron from the first dynode to the photocathode and its way back. The contribution of the late pulses as deduced from the plot are about 2.5 % in the "elastic" peak.

On the left side from the main peak, the pre-pulses contribution may be seen in the 10–15 ns preceding the main pulse. As expected, the contribution of the afterpulses is larger for the point like illumination which is directed toward the first dynode. In the same plot the dashed curve represents the Gaussian fit of the left side from the main peak.

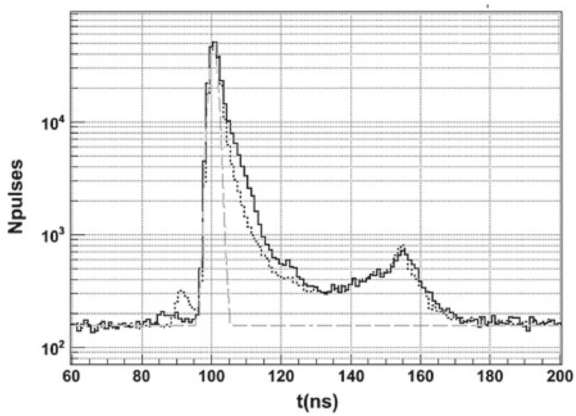

Fig. 2.11 Photon time arrival (transit time distribution) for the measurements in a dark room with the different sources: point-like illumination with laser (*dotted curve*), uniform illumination with laser plus diffuser (*continuous curve*). Delayed pulses with elastic peak at 145 ns are seen for both measurements. Prepulses at 95 ns are seen better for the point-like illumination. Gaussian fit of the left part of the spread functions is also shown (*grey dashed*)

In Fig. 2.12 the results from the measurements on the afterpulses are presented. One can see hits arriving shortly after the main hit (in 10–40 ns) or with a longer delay (6–8 μs). The total contributions of these afterpulses is 1.0 % and 0.8 % correspondingly. The late afterpulses (type 2) do not affect the track reconstruction of passing muons in the ANTARES detector but simply increase the light background. The fast afterpulses, instead, should be considered for the reconstruction algorithms. Also it can be seen that there is an increase of the afterpulses with a higher charge in respect to the charge distribution of single photoelectron hits (Fig. 2.10).

The obtained results are comparable with the measurements done during the PMT choice study (Aguilar et al. 2005). Similar measurements for the PMT used by the NEMO collaboration[3] (R7081) and the high quantum efficiency prototype of the same PMT are done during this thesis (Aiello et al. 2011).

2.1.4 Optical Module

The scheme of the optical module is shown in Fig. 2.13. It contains a PMT with its protection from the high pressure (glass sphere) and magnetic fields (metal cage) together with the PMT electronics and a calibration LED. The PMT is attached to the glass sphere via optical gel to reduce the unwanted reflection.

The protective envelope of PMT is a glass sphere of the kind routinely used by sea scientists for the buoyancy and for the instrument housing. These spheres, thanks to

[3] Now it is part of the KM3NeT project.

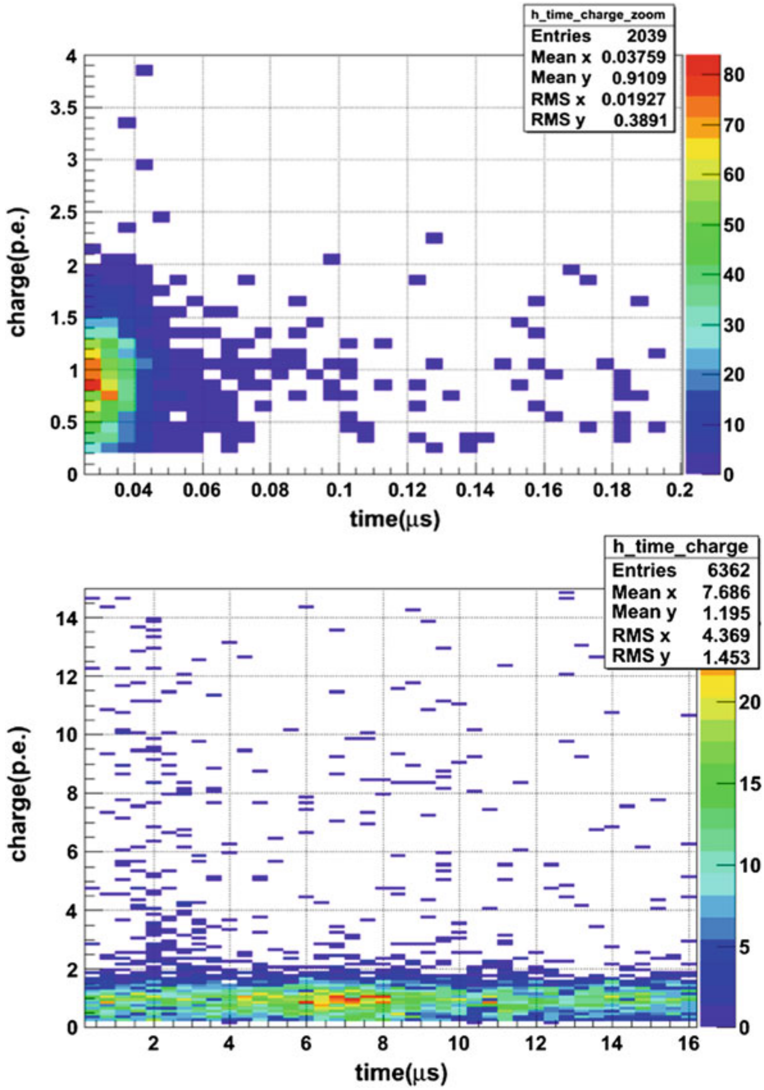

Fig. 2.12 Time versus amplitude distribution of afterpulses type 1 (*top*) and type 2 (*bottom*)

their mechanical resistance to a compressive stress and to their transparency, provide a convenient housing for photodetectors. Commercially available Vitrovex®17″ glass spheres were used.[4] The pressure qualification test allows the sphere usage till the depths of 7000 m.

[4]Nautilus Marine Service GmbH, http://www.nautilus-gmbh.de.

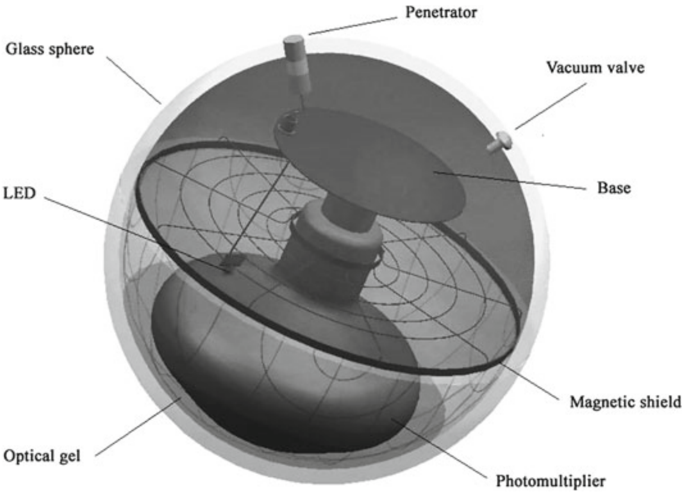

Fig. 2.13 Schematic view of the ANTARES OM and its components. The image is taken from Amram et al. (2002)

The PMT must be protected from the Earth's magnetic field which can deflect the electrons inside the tube and both reduce the PMT efficiency and affect the timing characteristics. The shielding was done with a hemispherical grid made of wires of μ-metal[5] closed by a flat grid on the rear of the bulb. The efficiency of the screening becomes larger as the size of the mesh is reduced and/or the wire diameter is increased, however the drawback is a shadowing effect on the photocathode. The compromise adopted by the ANTARES collaboration, a mesh of 68 mm^2 and wire diameter of 1.08 mm, results in a shadowing of less than 4 % of the photocathode area while reducing the magnetic field by a factor of three. Measurements performed in the laboratory show that this shielding provides a reduction of 0.5 ns on the TTS and a 7 % increase on the collected charge with respect to a naked, uniformly illuminated PMT (Ageron et al. 2011). The μ-metal cage is immersed in the gel and hold by it in the OM.

Instead of the passive PMT base provided by Hamamatsu, a new base (a modified version of the PHQ5912 base developed by ISEG[6]) was used. The high voltage and the distribution for the dynodes is generated by the base itself from the input 48 V used in ANTARES. Additional modification of the base were done to reduce the anode signal reflection.

On the rear part of the bulb of the PMT, a blue LED is glued in such a way to illuminate the pole of the photocathode through the aluminium coating. This LED is used to monitor the internal timing of the OM. A complete description of the ANTARES OM may be found in Amram et al. (2002).

[5] Sprint Metal, Ugitech, http://www.ugitech.com.

[6] ISEG Spezialelektronik GmbH, http://www.iseg-hv.com.

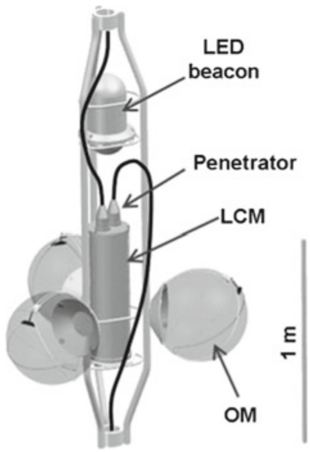

Fig. 2.14 Drawing of a storey equipped with 3 OMs which are connected to a local control module at the centre of the storey. The image is taken from Ageron et al. (2011)

2.1.5 Storey

Each OM is connected to a storey frame using a support system done with a titanium (Ti) wires, plate and bolts (Fig. 2.14). The storey frame hosts electronics for OM signal digitisation and transmission—Local Control Module (LCM). The LCM is placed in the titanium cylindrical container in the centre of the frame. A standard LCM contains the following elements:

Local Power Box Provides the 48 V for the optical modules and several different low voltages for the electronics boards. An embedded micro-controller allows the monitoring of the voltages, the temperatures and the current consumptions as well as the remote setting of the 48 V for the OMs. It is fed by the 400 V DC from the bottom of the line.

Clock The clock reference signal coming from shore reaches the bottom of the line where it is repeated and sent to each sector. Within a sector, the clock signal is daisy-chained between LCMs. The role of the clock card is to receive the clock signal from the lower LCM, to distribute it within the boards of the storey and to repeat it toward the upper LCM of the sector.

ARS boards The ARS motherboards host the front-end electronics of the OMs (one board per OM). This front-end electronics consists of a custom-built Analogue Ring Sampler (ARS) chip (Feinstein 2003) which digitises the charge and the time of the analogue signal coming from the PMTs.

DAQ/SC The Data Acquisition/Slow-Control card host the local processor and memory which are used to handle the data from the ARS chips and from the slow control, respectively. The processor has a fast Ethernet controller (100 Mb/s) that is optically connected to an Ethernet switch in the MLCM of the corresponding sector. The specific hardware for the readout of the ARS chips and data formatting is implemented in a high density field programmable gate array (FPGA).[7] The data are temporarily stored in a high capacity memory (64 MB SDRAM) allowing a de-randomisation of the data flow.

Compass board The compass motherboard hosts a TCM[8] sensor which provides heading, pitch and roll of the LCM. Those parameters are used for the reconstruction of the line shape and PMT positions.

Due to the segmentation of a line in sectors, one in five LCMs, called Master LCM (MLCM), acts as a master for other LCMs of the same sector and houses additional boards to collect electrical signals from the LCMs and convert them to the optical signal distributed to the bottom of the line.

The acoustic neutrino detection is integrated into ANTARES. The acoustic storeys are modified standard storeys with the PMTs replaced by acoustic sensors with custom-designed electronics for signal processing. The test system consists of six acoustic storeys with six acoustic sensors each. They are located on the last line of the detector and one additional instrumentation line. The detailed description may be found here (Aguilar et al. 2011a).

Several storeys also host light sources (LED optical beacons) which are used for time calibration (Sect. 2.3.1).

2.1.6 Line Infrastructure

Storeys are connected with a EMC which has three roles:

- optical data link: 21 single mode optical fibres
- power distribution: 9 electrical conductors
- mechanical link: breaking tension above 177 kN.

When subjected to a uniform horizontal sea current, as present at the ANTARES site, the 3-fold periodic symmetry of the storey induces a torque which is a function of the actual azimuth of the storey. The storey is in stable equilibrium when one of the three OMs is upstream of the current. Between two adjacent storeys, the EMC acts as a torsion spring tending to keep them at the same relative angle.

Each string is attached to its own Bottom String Structure (BSS). The function of the BSS is to anchor the line to the seabed with the capability of a recovery. The BSS is made of two parts: an unrecoverable dead weight laid on the seabed and a recoverable part sitting on top. The two parts are connected by a release system remotely controlled by acoustic signals. The dead weight is a horizontal square plate made of 50 mm thick carbon steel. The line stability requires a dead weight of 1270 kg in water, which means 1500 kg of steel.

The line is linked to the junction box by the interlink cable (IL), an electro-optical cable laying on the seabed and connected to the line at the level of the BSS by an

[7] Virtex-EXCV1000E, http://www.xilinx.com.

[8] PNI Sensor Corp., http://www.pnicorp.com.

underwater mateable connector, developed by the ODI company.[9] The remote line release implies an automatic disconnection system for the IL cable: the plug of the IL is fixed to the dead weight while the socket is located on the recoverable part of the BSS, at the end of a pivoting arm in such a way that it is extracted from the plug at the beginning of the ascent.

The BSS holds two lithium batteries powered transponders[10] in titanium cylinders which are equipped with release mechanism. The acoustic beacon capability of the transponders is employed in the Low Frequency Long Baseline (LFLBL) positioning and navigation system to monitor the position of the line anchor during its deployment and to determine its geodetic location with a precision of $\approx$1 m.

In addition to the release system, the BSS holds:

- a 1.8 m long titanium container housing the power module and the control electronics of the line
- a high resolution pressure meter, used for line positioning
- an acoustic transceiver at the top of a 3.6 m long rod of glass-epoxy, used as a reference emitter for the High Frequency Long Base Line (HFLBL) positioning system
- optional sound velocimeter, laser beacon, seismometer depending on the line
- a weight to keep the line vertical and under enough tension after release, even when the buoy reaches the sea surface.

The electronics container is the assembly of two cylinders similar to those of the LCMs. The power module part, at the top, contains transformers which deliver the five 400 V DC supplies needed for the sectors, starting from the 480 V AC provided by the junction box. An embedded micro-controller operates the remote powering of sectors. Voltages, temperatures and current consumptions are monitored. The micro-controller can also detect anomalies and is programmed to turn off the power in case of over-consumption. Like a standard LCM container, the control electronics cylinder houses a crate equipped with compass board, clock board and DAQ cards. There are boards which receives 20 MHz clock signal via an optical link from the shore and distribute it as electrical signal to the sectors. Also, the crate is equipped with a board which merges the optical signals from the sectors to distribute them through the single optical line. Each signal is sent to the shore by using a different laser colour.

2.1.7 Detector Infrastructure

The detector lines are connected with a Junction Box (JB) via interlink cables which is in turn connected to the shore using the main electro-optical cable. The JB is a

[9]Ocean Design Inc. (ODI), http://www.odi.com.

[10]Type RT 861 B2T; IXSEA/Oceano, http://www.ixsea.com.

pressure resistant titanium container mounted to the JB frame. The JB and its frame provide the following facilities:

- connection of the main electro optical cable and of the sea return power electrode
- power transformer housing
- line over-current protection system
- remote diagnostic system
- 16 electro-optical sockets to plug the interlink cables

The main electro optical cable (MEOC)[11] has been deployed from the site to the shore by a specialised cable-laying ship and crew under the responsibility of Alcatel. A standard undersea cable configuration with a single conductor was chosen to minimise the cable cost and weight. The use of the sea for current return reduces ohmic losses by a factor 4 compared with a cable sharing equivalent cross-section between supply and return conductors. The cable contains 48 monomode optical fibres in a stainless steel tube surrounded by "pressure vault" of two windings of steel armour wires. A tubular copper power conductor surrounds the vault and delivers current up to a maximum of 10 A to the junction box.

The onshore infrastructure consists of two separate buildings, the Shore Station housing control and data management infrastructure and providing space for onsite personnel, and the Power Hut devoted to power distribution requirements. The shore station is situated at La Seyne-sur-Mer. The building has three rooms dedicated to the operation of the ANTARES experiment: a computer room, a control room, and a service room. Computer room hosts racks for the clock crate, crates for the optical signal separation and the PC farm for data filtering and storage. The control room contains various computers for apparatus control and status monitoring.

The Power Hut is located near to MEOC landing point at Les Sablettes, and is connected to the latter with a fibre optical link 1.5 Km long. The Power Hut is connected to the 60 kVA, 400 V three-phase electrical distribution from Électricité de France. The building has been adapted to house the transformer 400/4000 V, the MEOC to shore link rack as well as the return current electrodes.

2.2 Data Acquisition

Data acquisition system (DAQ) (Aguilar et al. 2007) of ANTARES serves to digitise analogue signal of PMTs, transfer the data to shore, filter it and store it on the disks. The main concept chosen is "all data to shore". According to it the underwater part of the detector is performing only digitisation and all the filtering is done off-shore.

The presence of ^{40}K in the water and the bioluminescence introduces a lot of background signal which is not possible to store as raw data on disks for the long duration. For the first step the protection in the detector data filters against the bioluminescence bursts known as a high rate veto (HRV) is implemented. If a rate of a PMT exceeds

[11] Alcatel URC3 Type 4 (unrepeatered); Alcatel-Lucent, http://www.alcatel-lucent.com.

HRV value which is 400 kHz by default then the data from this PMT are not used. The same cutoff occurs when a PMT registers an excessive counting rate for a long period, overfilling the buffer (X_{off}). Lately, the filtering is done with triggers which have different purity and efficiency on the physics events (usually muons) detection. The filtered data is saved later on tapes which are accessible through the internet for any ANTARES participant.

2.2.1 Signal Digitisation and Data Transmission

A main digitisation method consists of the measurement of time at which negative anode signal passes a threshold (falling edge) and a charge integration over some time after the threshold. The threshold is typically set to 1/3 of the average peak signal and the time is fixed to 25 ns (which covers a length of most 1 p.e. signals). A combined charge-time information is called a level 0 (L0) hit. The signal is read-out and digitised by a custom application-specific integrated circuit, the analogue ring sampler (ARS) (Feinstein 2003). A local clock in ARS is used for the determination of the hit time arrival. The time resolution of the system is better than 0.4 ns. An ARS after digitisation of a signal has an about 225 ns dead time. Each PMT is connected to a pair of ARS readouts which are activated by a token passing through the token ring between these ARS. It takes about 13 ns to pass the token so during this time the PMT signal is not elaborated. The timeline of this process is shown in Fig. 2.15.

Three PMTs have in total 6 ARS which are connected to a FPGA placed in the storeys local control module (LCM). FPGA arranges hits produced by each ARS in a time window of 104.8 μs to a separate data frame. A 20 MHz clock generated off shore is used to provide a common time for each ARS. These clocks are synchronised with a master clock through the optical fibre network. A scheme of these LCM components is shown in Fig. 2.16. The master clock is in turn synchronised to the GPS time with an accuracy of ~100 ns (Aguilar et al. 2011b). This time affects only the absolute neutrino arrival time and it is negligible in respect to the Earth rotation period.

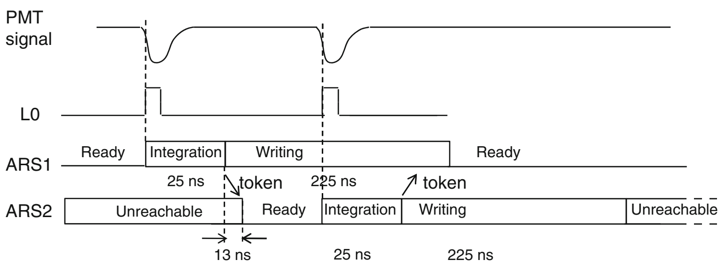

Fig. 2.15 Timeline of two consecutive PMT pulses and the corresponding occupancy in the front-end electronics. The image is taken from Aguilar et al. (2010)

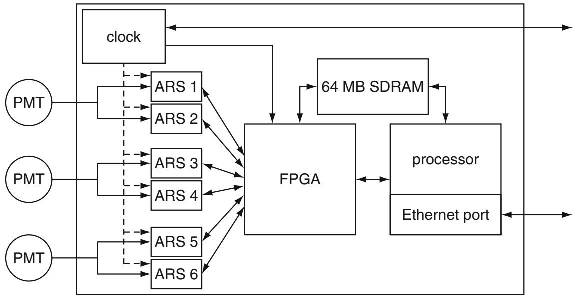

Fig. 2.16 Schematic picture of the main hardware components in the electronics module of a storey Aguilar et al. (2007)

Transmission Control Protocol and Internet Protocol (TCP/IP) together with ControlHost package is used for communication and data transfer (Gurin and Maslennikov 1995). The ControlHost requires a server which is placed in the control room and clients which send and receive the data through the server to another clients using tags. Each LCM has a processor which runs vxWorks operating system[12] with a DaqHarness program which sends the data, collected from each ARS to a ControlHost server. The server distributes the data to the DataFilter clients which group the data by the time organising the data time slices of 104.8 μs from the data frames. Once a time slice is ready, it is processed by its DataFilter with a trigger software. The filtered data is sent in turn to the ControlHost server which forwards it to a DataWriter process that writes it to the disk. At the end the data from the local discs is transferred to the Lyon computing centre through the Internet and stored on tapes.

2.2.2 Data Filtering and Storage

All the digitised signals from PMTs are transferred to the shore. The total data output is about 0.3–0.5 GB/s during low bioluminescence periods. This high data flow contains mostly the optical background and so it needs to be filtered before the storage. The filtering is done with different trigger algorithms which are designed to detect signal from particles in the detector by the space-time correlation between hits (de Jong 2005). These trigger algorithms are implemented in the DataFilter program which triggers PMT hits and produces Physics Events containing all data in a window (-2.2, 2.2 μs) from the triggered hits. This time window covers well a muon passage time through the detector.

All the collected hits are called level 0 hits (L0) hits in ANTARES detector. They are mostly coming from the optical noise. The first level cut searches for coincidences between the hits in the LCM between the 3 PMTs which are very close to each other. It assumes that the Čerenkov light coming from muons should hit the nearby PMTs. A distance between PMT centres in LCM is about 0.7 m. The time window chosen is

[12]http://www.windriver.com.

20 ns which is much more than sufficient to detect scattered hits. The rate of so-called L1 hits per PMTs pair can be estimated as:

$$f_{L1} = 2\tau f_{L0}^2 \sim 2 \times 20 \times 10^{-9} \times (100 \times 10^3)^2 \sim 400 \text{ Hz}, \tag{2.1}$$

assuming $f_{L0} = 100$ kHz L0 rate per PMT. The number of PMT in LCM is three so the number of pairs is also three. This means the rate of the L1 hits is at least two orders of magnitude lower than the L0 rate in the detector. Additionally, the single hits with a charge of more than 3 p.e. are added to the L1 hits. The background in these hits is mainly due to afterpulses which rate is about 0.18 % (from Fig. 2.12).

The second level triggers are applied mostly on L1 hits searching clusters (L2 hits) and checking the compatibility with different track directions. Clusters are formed by the hits connected with a so-called causality relation, which is the following for the two hits (t_i, r_i) and (t_j, r_j):

$$|t_i - t_j| \leq |\bar{r}_i - \bar{r}_j|/v_g + \tau, \tag{2.2}$$

where $v_g = c/n$ is the group velocity of light in the water and τ takes to account a dispersion and PMTs position uncertainties. There are several triggers developed by the ANTARES collaboration. They have different efficiency on the neutrino detection and a different event purity. The triggers which are used for the data taking are set for each run separately depending on the optical background conditions. The main strategy is to have a final detector event rate of order of 100 Hz which produces about 1 GB of physics events per 1–2 h of data taking.

2.3 Detector Calibration

The detector calibrations are important for the event reconstruction precision. The calibration details are written to the database as a calibration set. There are two types of sets—sets which are used for the online detector work (these are needed for the triggering) and more precise offline calibrations are using the data already collected (these are used for the event reconstruction).

2.3.1 Time Calibration

The time calibration in ANTARES is described in details in Aguilar et al. (2011b). Before the deployment of the detector strings the preliminary time calibration is done in laboratory. After the deployment an optical beacons system (OB) is used for the calibration adjustments (Ageron et al. 2007). The four LED optical beacons which emit the blue light are placed in each detector line on the sectors 2, 9, 15 and 21 (counted from the bottom to the top). Each of the OB has its small PMT close to the LEDs to know precisely the light emission start. Several flashes are done with the OB and the time residual between the OB emission and the PMT is measured for each PMT on the 7 storeys above the OB excluding the first one which is too close to the OB. The peak time of the time residual distribution is compared with the time expected from the light propagation and the calibrations done before the deployments. After the adjustments are done if it is needed.

An independent cross check of the inter calibration between the OMs in the same storey are done with the Čerenkov light from a potassium decay. There are about 150 photons from each decay which can be simultaneously seen in both OMs. If one plots the time difference between all hits for the pair of OMs a Gaussian peak of 10 ns FWHM from the ^{40}K emerges above the random background as it is seen in Fig. 2.17. Its mean should be at 0 if the time calibration is perfect.

There are two laser beacons which are used for the calibration of the time offsets between the lines. The laser beacons are powerful light sources which are placed on the bottom of two lines. The detected light on the other strings is compared with the estimated one from the line positions and the calibrations in the laboratory.

These time calibrations are performed regularly by the detector operators and then the calibration sets are created by the calibration experts. The current calibration scheme attains the relative time calibration between the detector elements of less than 1 ns.

2.3.2 Charge Calibration

Each ARS produces an integrated charge as a number of amplitude to voltage converter (AVC) channels. This is needed to be converted to a number of photoelectrons. For this a charge corresponding to one photon is needed to be measured together with the charge measured in the absence of the signal (pedestal) (Baret 2009). Both measurements are done regularly in-situ with the optical background which is mostly a

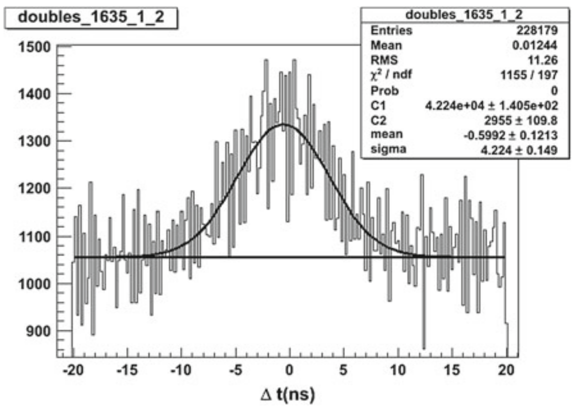

Fig. 2.17 An example of distribution of the time residual between hits on two PMTs

single photon signal. A 1 p.e. charge distribution is measured by writing the charge of all hits with a 0.3 p.e. threshold. A 0 p.e. charge distribution is obtained by integrating the charge at some random start time. Both obtained distributions are fitted with a Gaussian function and mean values are extracted. Using these values a charge in photoelectrons for any hit can be calculated as:

$$Q = \frac{AVC - AVC_{0\text{p.e.}}}{AVC_{1\text{p.e.}} - AVC_{0\text{p.e.}}} \tag{2.3}$$

where AVC is the measured charge in AVC channels, $AVC_{0\text{p.e.}}$ and $AVC_{1\text{p.e.}}$ are obtained 0 and 1 p.e. means from the calibrations.

If the pulse has an amplitude just above the threshold its time cannot be identified correctly by ARS and a zero value is produced. This hits do not affect the detector operation but may be used for the threshold tuning. Selecting time 0 hits it is possible to know the charge of the hits with an amplitude of the threshold set. The threshold can be tuned then for each ARS to 1/3 p.e. The values of effective thresholds, 0 and 1 p.e. changes with time and especially during the high voltage tunings which are done to have similar charge output for each PMTs. The above mentioned PMT parameters are monitored regularly and stored in the DataBase.

2.3.3 Position Calibration

The positions of the line anchors on the sea bed are well known and stable in time. The absolute positioning of each anchored detector component is calculated with an accuracy of about 1 m by acoustic triangulation from the surface with a ship equipped with a differential GPS. However the lines move freely in the water due to the current

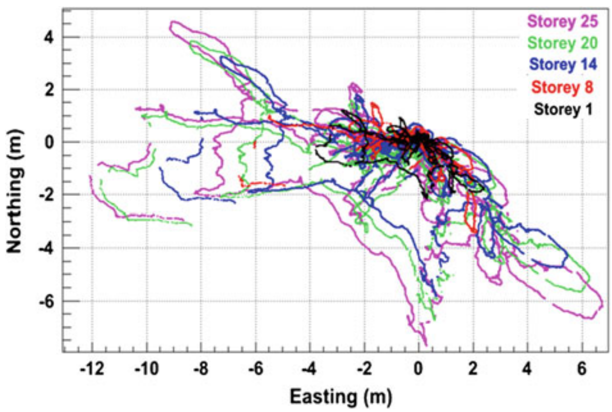

Fig. 2.18 The horizontal displacement of the hydrophones on one of the lines with respect to the anchor for a 6 months period

and the photomultipliers, especially on the top of the detector, change their absolute position and orientation. Their position is monitored by the system of the acoustic transponders and receivers distributed over the lines and on the sea bed (Adrián-Martínez et al. 2012). There are transmitters installed at the anchor of each line. Acoustic detectors—hydrophones are mounted on the storeys 1, 8, 14, 20 and 25 to detect signals in 40–60 kHz range. The distances are obtained by the triangulation of each receiver with respect to the emitters. This procedure is done regularly and the data is stored in the database. A relative movement of one of the detector lines is shown in Fig. 2.18. The LCM orientations are measured by compasses and tiltmeters in each storey. The current positioning strategy allows to monitor relative positions of all of the optical modules with an accuracy better than 20 cm.

References

S. Adrián-Martínez et al., The positioning system of the ANTARES Neutrino Telescope. JINST **7**(8), 1 (2012). T08002, ISSN 1748–0221, http://iopscience.iop.org/1748-0221/7/08/T08002/

M. Ageron et al., The ANTARES optical beacon system. NIM A **578**(3), 498–509 (2007). ISSN 01689002, http://linkinghub.elsevier.com/retrieve/pii/S0168900207012041

M. Ageron et al., ANTARES: the first undersea neutrino telescope. NIM A **656**(1), 11–38 (2011). ISSN 01689002, http://linkinghub.elsevier.com/retrieve/pii/S0168900211013994

J. Aguilar et al., Study of large hemispherical photomultiplier tubes for the ANTARES neutrino telescope. NIM A **555**(1–2), 132–141 (2005). ISSN 01689002, http://linkinghub.elsevier.com/retrieve/pii/S016890020501836X

J. Aguilar et al., The data acquisition system for the ANTARES neutrino telescope. NIM A **570**(1), 107–116 (2007). ISSN 01689002, http://linkinghub.elsevier.com/retrieve/pii/S0168900206017608

J. Aguilar et al., Performance of the front-end electronics of the ANTARES neutrino telescope. NIM A **622**(1), 59–73 (2010). ISSN 01689002, http://linkinghub.elsevier.com/retrieve/pii/S0168900210014154

J. Aguilar et al., AMADEUS—the acoustic neutrino detection test system of the ANTARES deep-sea neutrino telescope. NIM A, 626–627 (2011a). 128–143, ISSN 01689002, http://linkinghub.elsevier.com/retrieve/pii/S0168900210020772

J. Aguilar et al., Time calibration of the ANTARES neutrino telescope. Astropart. Phys. **34**(7), 539–549 (2011b). ISSN 09276505, http://linkinghub.elsevier.com/retrieve/pii/S0927650510002367

S. Aiello et al., The measurement of late and after-pulses in the large area Hamamatsu R7081 photomultiplier with improved quantum-efficiency photocathode, Technical report, INFN/TC-04/11 (2011)

P. Amram et al., The ANTARES optical module. NIM A **484**(1–3), 369–383 (2002). ISSN 01689002, http://linkinghub.elsevier.com/retrieve/pii/S0168900201020265

B. Baret, Charge calibration of the ANTARES high energy neutrino telescope, in Proceedings of the 31st ICRC, (ódź, 2009) http://icrc2009.uni.lodz.pl/proc/pdf/icrc1184.pdf

F. Feinstein, The analogue ring sampler: a front-end chip for ANTARES. NIM A **504**(1–3), 258–261 (2003). ISSN 01689002, http://linkinghub.elsevier.com/retrieve/pii/S0168900203007733

R. Gurin, A. Maslennikov, Controlhost: distributed data handling package, Technical report (1995) http://www.nikhef.nl/pub/experiments/antares/software/Dispatcher/ControlHost.ps

M. de Jong, The ANTARES Trigger Software, Technical report ANTARES-SOFT-2005-005 (2005)
B. Lubsandorzhiev et al., Photoelectron backscattering in vacuum phototubes. NIM A **567**, 12–16 (2006). ISSN 01689002, http://linkinghub.elsevier.com/retrieve/pii/S0168900206008606
D. Palioselitis, Measurement of the atmospheric neutrino energy spectrum, Ph.D. thesis, (Institute for High Energy Physics (IHEF), 2012) http://dare.uva.nl/cgi/arno/show.cgi?fid=444188

http://www.springer.com/978-3-319-20411-6

Neutrino Astrophysics with the ANTARES Telescope
Kulikovskiy, V.
2015, XIII, 119 p. 85 illus., 34 illus. in color., Hardcover
ISBN: 978-3-319-20411-6